Enhanced Charge Transport in 2D Perovskite Solar Cells via Fluorination of Organic Cation

Fei Zhang,[1+] Dong Hoe Kim,[1+] Haipeng Lu,[1] Ji-Sang Park,[2] Bryon W. Larson,[1] Jun Hu,[3] Liguo Gao,[1, 4] Chuanxiao Xiao,[1] Obadiah G. Reid,[1,6] Xihan Chen,[1] Qian Zhao,[1] Paul Ndione,[1] Joseph J. Berry,[1] Wei You,[3] Aron Walsh,[2,5] Matthew C. Beard,[1] Kai Zhu[1,*]

[1] National Renewable Energy Laboratory, Golden, Colorado 80401, United States

[2] Department of Materials, Imperial College London, London SW72AZ, United Kingdom.

[3] University of North Carolina at Chapel Hill, Chapel Hill, North Carolina 27599, United States

[4] School of Petroleum and Chemical Engineering, Dalian University of Technology, Panjin, P. R. China

[5] Department of Materials Science and Engineering, Yonsei University, Seoul 03722, Korea

[6] Renewable and Sustainable Energy Institute, University of Colorado Boulder, Boulder, Colorado 80309, USA

[+] These authors contribute equally.

Correspondence and requests for materials should be addressed to K.Z. (email: Kai.Zhu@nrel.gov)

Abstract

Organic-inorganic halide perovskites incorporating two-dimensional (2D) structures have shown promise for enhancing the stability of perovskite solar cells (PSCs). However, the bulky 2D cations often limit charge transport. Here, we report on a simple approach based on molecular design of the organic 2D spacer to improve the transport properties of 2D perovskites, and we use phenethylammonium (PEA) as an example. We demonstrate that by fluorine substitution on the para position in PEA to form 4-fluoro-phenethylammonium (F-PEA), the average phenyl ring centroid-centroid distances in the organic layer become shorter with aligned stacking of perovskite sheets. The impact is enhanced orbital interactions and charge transport across adjacent inorganic layers as well as increased carrier lifetime and reduced trap density. Using a simple perovskite deposition at room temperature without using any additives, we obtained power conversion efficiency >13% for $(F\text{-}PEA)_2MA_4Pb_5I_{16}$ based PSCs. In addition, the thermal stability of 2D PSCs based on F-PEA is significantly enhanced compared to those based on PEA.

Introduction

Three-dimensional (3D) perovskites (e.g., $CH_3NH_3PbI_3$ or $MAPbI_3$) were initially reported as a sensitizer with a power conversion efficiency (PCE) of 3.8% in 2009.[1] In a rapid evolution, the PCE of perovskite solar cells (PSCs) has reached 23.3% within 9 years.[2-4] In addition to the continuous effort to improve cell efficiencies, recent work has been devoted to improving the long-term stability of PSCs against moisture, heat, and light for practical applications.[5]

Unlike small cations (e.g., MA^+) in 3D perovskite films, the bulky organic cations in two-dimensional (2D) perovskites (e.g., phenethylammonium (or PEA^+) and butylammonium (or BA^+)) form discrete sheets of lead halide octahedra sandwiched between organic spacer layers and can provide steric hindrance for surface water adsorption in the initial step of decomposition.[6] The hydrophobic bulky alkylammonium cations in 2D perovskite lattices can effectively block the accessible pathways of moisture invasion.[7] The 2D perovskite is generally described as $M_2A_{n-1}B_nX_{3n+1}$, where M is a large organic cation, such as BA and PEA; A is normally methylammonium (MA), formamidinium (FA), or Cs; B is normally Pb or Sn; X is a halide anion, namely, I, Br, or Cl; and n is the number of layers of metal halide sheets. Note that in the literature the n values are normally calculated based on the composition of the precursor solutions. Despite improved stability, perovskites with primarily 2D crystal structures are generally not good options for high-performance solar cells because of their reduced and anisotropic charge transport associated with the bulky organic spacers.[6]

One approach in addressing the transport issue is to lower the ratio of intercalated large cations that form the 2D perovskite lattice.[8,9] For example, by optimizing the amount of PEAI into MAI and PbI_2 solution, the n value in $PEA_2MA_{n-1}Pb_nI_{3n+1}$ compounds can in theory be adjusted from 1 to ∞.[8] Following this strategy, a certified PCE of 15.3% was achieved with $PEA_2MA_{n-1}Pb_nI_{3n+1}$ ($n = 60$).[8] However, with a large n value (normally when $n > 6$), the resulting structure is essentially a 3D perovskite with a small amount of 2D components incorporated as a dopant.[6] Another approach is to facilitate the preferred vertical growth orientation of the 2D perovskites by either using additives (e.g., NH_4SCN,[10-12] MACl,[13-15] and NH_4Cl[11]) or hot-casting at an elevated deposition temperature,[16-19] and such approaches have resulted PCEs greater than 10%. However, for the hot-casting growth, it is difficult to precisely control the substrate temperature during spin-coating; thus, it is not ideal for device reproducibility.

The primary motivation for pursuing a more-oriented growth of the 2D perovskites is to facilitate charge transport/collection across the 2D perovskite absorber layer. In this work, we report on a different approach—chemically modifying the bulky organic spacer to improve the out-of-plane transport. Fluorine substitution on the para position in PEA forms 4-fluoro-phenethylammonium (F-PEA) and we find that the average ring centroid-to-centroid distances in the organic layer is reduced. This enhances the orbital interactions between the inorganic layers, leading to more efficient charge transport across adjacent inorganic layers. The simple fluorination of PEA cations also enhances the stacking alignment of the perovskite sheets allowing for better interlayer electronic coupling. When using F-PEA in n=5 2D perovskite—i.e., $(F\text{-}PEA)_2MA_4Pb_5I_{16}$)—the perovskite films exhibit faster charge transport, longer carrier lifetimes, and a lower trap density compared to the PEA-based analogue with no fluorine. As a result, we obtain a PCE > 13% for $(F\text{-}PEA)_2MA_4Pb_5I_{16}$-based PSCs prepared without using any additives and fabricated at room temperature. These devices also show a better thermal stability than that of $(PEA)_2MA_4Pb_5I_{16}$. This promising approach provides a simple route for designing 2D PSCs with high efficiency and stability.

Result and Discussion

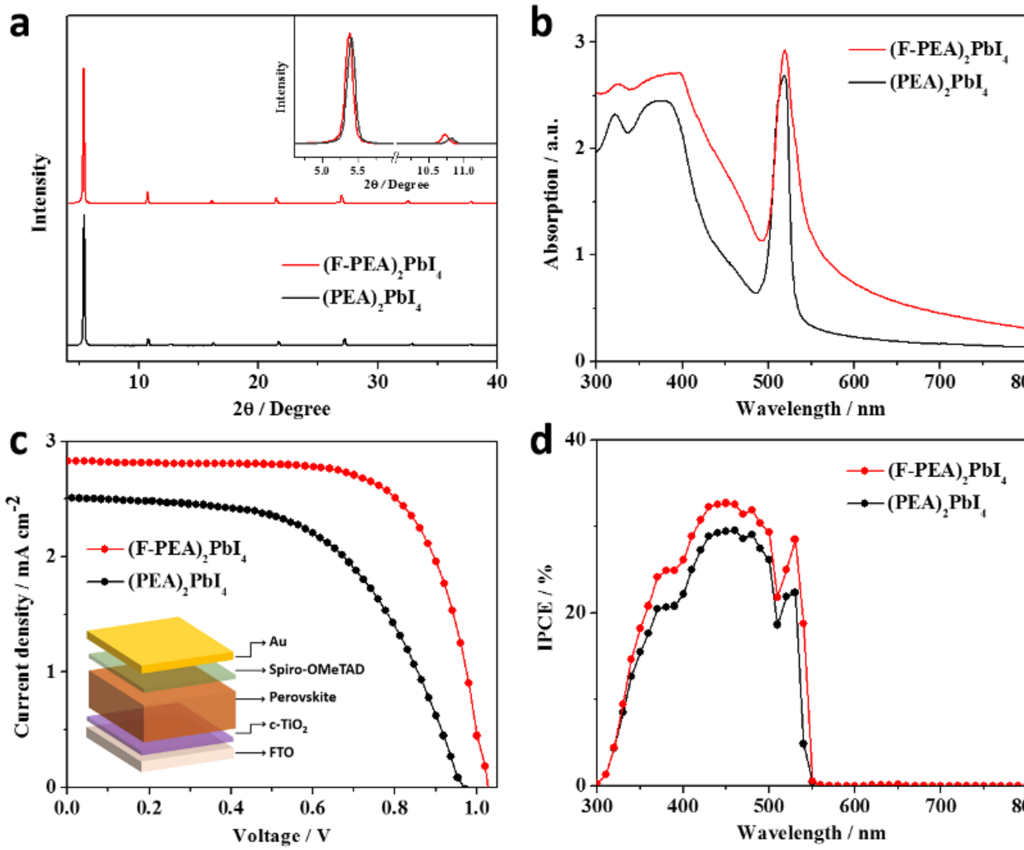

Figure 1. (**a**) XRD patterns and (**b**) UV-vis absorption spectra of n=1 2D $(PEA)_2PbI_4$ and (F-PEA)$_2PbI_4$ perovskite thin films. (**c**) J–V curves and (**d**) IPCE spectra of perovskite solar cells based on $(PEA)_2PbI_4$ and (F-PEA)$_2PbI_4$. The J–V) curves were measured with forward scan with a bias step of 10 mV.

Figure 1a shows X-ray diffraction (XRD) patterns of perovskite thin films based on n=1 2D $(PEA)_2PbI_4$ and (F-PEA)$_2PbI_4$, with the growth planes primarily parallel to the substrate. In comparation to $(PEA)_2PbI_4$, the scattering of X-rays of (F-PEA)$_2PbI_4$ displays a slight shift towards smaller angles; the inset of **Figure 1a** shows the zoom-in view of the first two diffraction peaks. Based on the (002) reflection peaks, the distance between the 2D perovskite layers is calculated to be 16.41 Å and 16.35 Å for (F-PEA)$_2PbI_4$ and $(PEA)_2PbI_4$, respectively. The optical ultraviolet-visible (UV-vis) absorption spectra (**Figure 1b**) are typical of 2D perovskites, with a high-energy continuum absorption edge and a lower-energy excitonic peak. The slight increase in the absorbance for F-PEA is likely due to increased scattering. To compare how the different organic cations affect the photovoltaic (PV) properties, we fabricated planar PSCs in a configuration of

FTO/compact-TiO_2/perovskite/spiro-OMeTAD/Au. **Figure 1c** shows the photocurrent density–voltage (J–V) curves of (F-PEA)$_2$PbI$_4$- and (PEA)$_2$PbI$_4$-based PSCs under an AM 1.5G solar simulator. The (PEA)$_2$PbI$_4$-based PSC gives a PCE of 1.34%, with a short-circuit current density (J_{sc}) of 2.51 mA cm^{-2}, open-circuit voltage (V_{oc}) of 0.97 V, and fill factor (FF) of 0.55. In contrast, the (F-PEA)$_2$PbI$_4$-based PSC yields an PCE of 1.90%, with improvements from all PV parameters (J_{sc} = 2.83 mA cm^{-2}, V_{oc} = 1.02 V, and FF = 0.66); this is among the highest PCE obtained, thus far, for n=1 2D lead-iodide-based PSCs. **Figure 1d** shows the incident photon-to-current efficiency (IPCE) spectra, from which the integrated current densities were found to be 2.39 mA/cm^2 and 2.69 mA/cm^2 for (PEA)$_2$PbI$_4$ and (F-PEA)$_2$PbI$_4$ PSCs, respectively. Note that the significant PCE improvement is primarily caused by the increase of FF (by ~20%) when PEA is replaced with F-PEA, which likely results from the improvement in the charge-transport property.

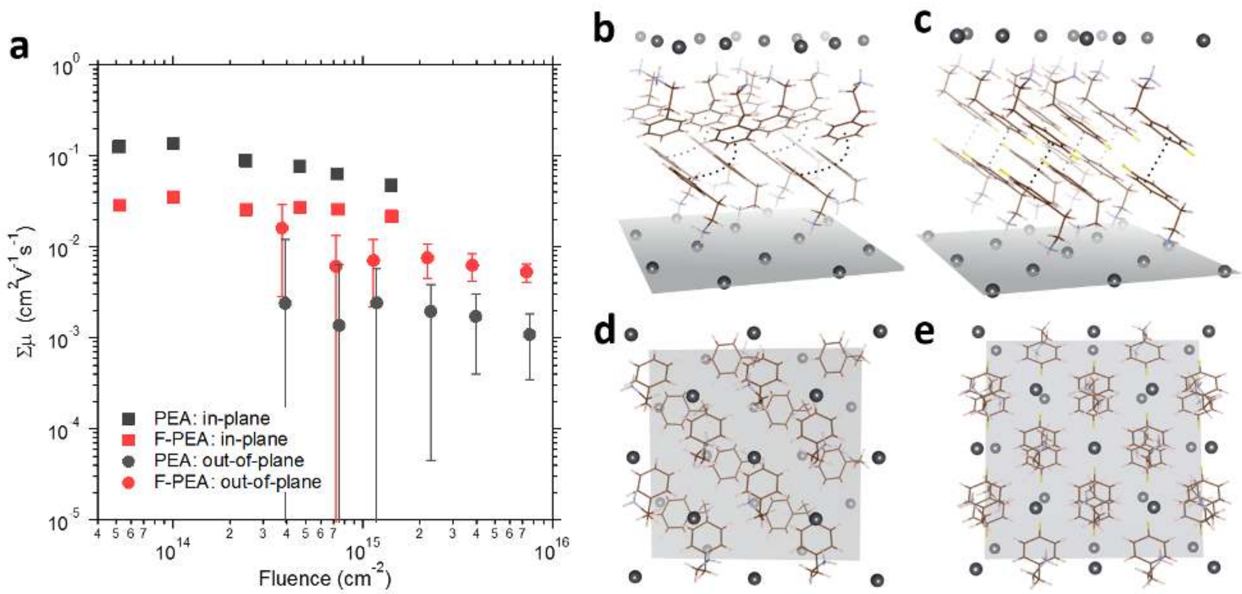

Figure 2. (**a**) TRMC comparison of out-of-plane and in-plane transport for n=1 2D perovskite thin films. The results are calibrated by the internal quantum yield of charges as discussed in text. The structures of (**b,d**) (PEA)$_2$PbI$_4$- and (**c,e**) (F-PEA)$_2$PbI$_4$-based on single crystal XRD.[20]

We use time-resolved microwave conductivity (TRMC)[21,22] measurements to compare in-plane and out-of-plane transport in pure (n=1) 2D perovskite thin-films of (PEA)$_2$PbI$_4$ and (F-

$PEA)_2PbI_4$. This is achieved using two different microwave cavity configurations that orient the perovskite layers either parallel or perpendicular to the microwave field, whilst the optical excitation axis remains perpendicular to the film (details given in the Experimental Section in SI). For n=1 2D perovskite films, the 2D plane is usually parallel to the substrate (**Figure 1a**; XRD comparison of n=1 2D perovskite thin films), making substrate/film orientation a good method for controlling the orientation of the perovskite layers in the microwave field.

Figure 2a shows the 9 GHz mobility extracted from the TRMC data, using the internal quantum yield of charges calculated from the device data in **Figure 1b,d**. Details of this calculation are given in SI. The out-of-plane (or inter-sheet) microwave mobility of $(F\text{-}PEA)_2PbI_4$ is ~7x larger than that of $(PEA)_2PbI_4$. However, based on the XRD results, the interlayer distance in the F-PEA film appears to be slightly larger than the PEA film, suggesting that the improved out-of-plane conductivity is not simply determined by the interlayer distance, as previously reported.[13] **Figure S4** shows a similar countervailing example, comparing $(BA)_2PbI_4$ to $(PEA)_2PbI_4$. The layer-to-layer distance for $(BA)_2PbI_4$ is shorter (13.76 Å) than $(PEA)_2PbI_4$ (16.35 Å), but the out-of-plane mobility is slightly smaller.

This observation is not too surprising if we consider charge transport between inorganic layers as a tunneling process mediated by the organic interlayer. There are two co-equal properties of a tunnel junction that control the tunneling probability: distance, and barrier height. The latter is much more complex and difficult to predict than the former but could turn out to be more important here, where the fractional change in interlayer distance among all the organic cations we have investigated is small. Differences in barrier height/structure could arise here due to two main effects: (1) a change in the intermolecular electronic coupling between neighboring organic cations, and (2) a change in the energetic alignment between the perovskite transport bands and the oxidation or reduction potential of the organic cation. For example, we predict that interlayer hole transport would be optimized when the oxidation potential of the organic cation is resonant with the valence band of the perovskite layer *and* cations from neighboring layers possess large intermolecular electronic coupling integrals between highest occupied molecular orbitals

(HOMOs). At this time, we do not possess any data that allows us to evaluate the question of energetic alignment of the various cations with the perovskite band structure, which will be a focus of future work. However, there is ample structural data in **Figure 2b–e** to evaluate the likely influence of intermolecular coupling.

Using fluorine substitution to direct and enhance intermolecular packing is a strategy often reported in organic solar cells to enhance PV performance because it enhances mobility as a result of planarization of the polymer/molecular backbone along with better intermolecular order,[23-25] and preferential orientation of the backbone with respect to the discrete donor/acceptor interface.[26] Here, fluorine substitution in the organic layer also affects the intermolecular packing, as well as, the electronic interactions. **Figure 2b–e** shows the side and top views for both samples relative to the 2D sheets of PbI_6 octahedra; only the lead atom centers of the octahedra are shown for clearer visualization of the organic layer.[20] We have also added a grey plane through one layer of lead atoms for visual reference, which is positioned in the background of the top-view figures. Analysis of the single-crystal XRD data for each structure reveals several key differences. First, the phenyl rings are parallel slip-stacked in the F-PEA structure *vs*. edge-to-face stacked in the PEA structure (**Figure 2b,c)**. The co-facial inter-ring plane distance in the F-PEA sample is 3.588 Å, which corresponds to a maximum van der Waals attraction distance for a parallel stacked aromatic dimer.[27] In the PEA sample with edge-to-face stacking, there are four different closest ring-to-ring distances that all correspond to the nearest hydrogen atom of an "edge" ring to the centroid of a "face" ring. These values are 3.009 Å, 3.050 Å, 3.078 Å, and 3.122 Å, suggesting that these are more likely steric interactions rather than electrostatic. For ring centroid-to-centroid distances ($R_{\text{cen-cen}}$), there are eight unique nearest-neighbor $R_{\text{cen-cen}}$ values ranging from 4.892–6.770 Å in the PEA sample, compared to four unique $R_{\text{cen-cen}}$ values ranging from 3.878–6.709 Å in the F-PEA sample. Thus, it is extremely probable that there is enhanced π-π overlap in F-PEA relative to PEA which could reduce the barrier height and facilitate more-efficient charge transport.[28,29]

The different arrangements of the PEA and F-PEA molecules were also found in density functional theory calculations (**Figure S5**). To find out which arrangement the molecules prefer, we calculated how much the energy changes from molecular edge-to-face stacking to the parallel arrangement. The energy change (ΔE_f) was obtained with and without dispersion correction to check the effect of the van der Waals interaction. PEA molecular layers prefer to be stacked edge-to-face regardless of the inclusion of the dispersion correction (**Table S2)**. F-PEA molecules, on the other hand, are calculated to be stacked in parallel (ΔE_f = -0.05 eV/f.u.) when the dispersion interactions are included. The edge-to-face stacking is slightly favored (ΔE_f = 0.01 eV/f.u.) in the absence of long-range interactions. This result confirms that the van der Waals interaction promotes the parallel arrangement of phenyl rings. We expect that one arrangement will be dominant for each material because of the noticeable energy difference between the two arrangements.

It is noteworthy that the sheet-to-sheet position of lead octahedra centers are also different between the two samples. The PEA molecules are oriented edge-to-face, so the coordinating amine groups are also offset relative to each other at the top and bottom of the organic layer, meaning that the Pb centers also end up staggered in alternating sheets (refer to the lead atom and NH_2 positions in the top views of **Figure 4d,e**). In the F-PEA sample, the rings are parallel slip stacked and offset relative to the plane of the lead atoms, allowing the amine groups to be approximately eclipsed in the vertical direction; hence, the lead atoms are also in an eclipsed orientation between sheets. The simple fluorination of PEA cations aligns the stacking of perovskite sheets and allows for a better interlayer electronic coupling, which is better for charge transfer.[30,31] As such, we attribute the enhanced out-of-plane conductivity in the F-PEA sample to the preferred molecular stacking in both organic (reduced ring-to-ring distance) and inorganic phases (aligned PbI_6 sheets). Interestingly, according to the in-plane *vs*. out-of-plane TRMC results for the n=1 2D samples, the non-substituted PEA sample exhibits a higher in-plane carrier mobility. We hypothesize that the in-plane mobility is more heavily determined by the Pb planes rather than the organic layer.[31]

We further extended our comparison study to n=5 2D perovskites using PEA and F-PEA. 2D perovskites with n=4 or 5 have recently received increasing attention as potential candidates for achieving high stability as well as high efficiency for solar cells.[8,32] **Figure S6** displays schematic crystal structures of $(F\text{-}PEA)_2MA_4Pb_5I_{16}$ and $PEA_2MA_4Pb_5I_{16}$. F-PEA (or PEA) based n=5 2D perovskite films were prepared from precursor solutions consisting of PbI_2, F-PEAI (or PEAI), and CH_3NH_3I (MAI) at a stoichiometric ratio of 5:2:4 in dimethyl formamide (DMF) and dimethyl sulfoxide (DMSO) with a concentration of 1.25 mol/L. The coating process was done in air and detailed procedures are given in SI. We investigated the surface morphology of 2D perovskite films by scanning electron microscopy (SEM) and atomic force microscopy (AFM) (**Figures S7 and S8**). Both films appear uniform and the presenting surface morphology of $(F\text{-}PEA)_2MA_4Pb_5I_{16}$ has larger structures than that of the $(PEA)_2MA_4Pb_5I_{16}$ film, and the $(F\text{-}PEA)_2MA_4Pb_5I_{16}$ film clearly presents a more homogenous cross-section consistent with fewer internal boundaries. XRD patterns (**Figure S9**) exhibit similar, strong, and sharp perovskite characteristic peaks. The intensity of the $(F\text{-}PEA)_2MA_4Pb_5I_{16}$ perovskite film at the (110) peak becomes stronger and the full width at half-maximum (FWHM, 0.26°) decreased when compared with the $(PEA)_2MA_4Pb_5I_{16}$ perovskite films (0.29°). Although determination of grain size is difficult for this class of materials, these data indicate that the reduced FWHM is consistent with the morphology changes viewed in the SEM/AFM. UV-vis absorption spectra (**Figure S10**) of $(F\text{-}PEA)_2MA_4Pb_5I_{16}$ and $(PEA)_2MA_4Pb_5I_{16}$ thin films display various excitonic absorption peaks associated with different n values, which are consistent with previous reports.[8-15]

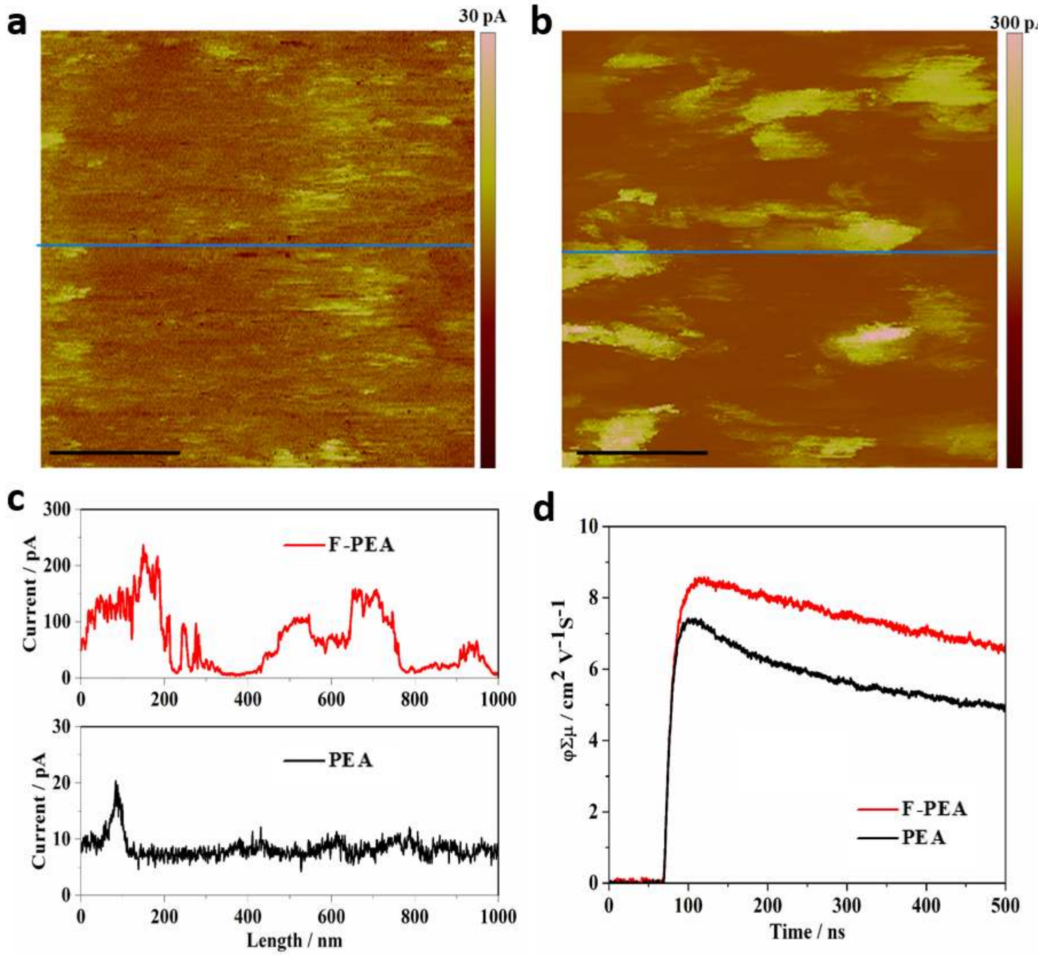

Figure 3. The C-AFM mapping images for the n=5 2D perovskite films based on (**a**) PEA and (**b**) F-PEA obtained at a bias voltage of 1 V in the dark. The scale bar is 300 nm. (**c**) The line profiles of current mapping of the corresponding perovskite films. (**d**) Typical photoconductivity ($\varphi\Sigma\mu$) transient for the corresponding perovskite films.

To examine the impact of fluorination of PEA on the optoelectronic properties in n=5 2D perovskites, we carried out a set of characterizations including conductive atomic force microscopy (C-AFM), TRMC and time-resolved photoluminescence (TRPL) spectroscopy. As shown in **Figure 3a,b**, the $(PEA)_2MA_4Pb_5I_{16}$ sample shows relatively low current signal, which indicates poor electrical conductivity of the perovskite films. In contrast, the $(F\text{-}PEA)_2MA_4Pb_5I_{16}$ sample displays a significantly increased (about 10-fold) current signal, which suggests better carrier conduction. This drastic difference is further illustrated in the line-profile comparison of the C-AFM results (**Figure 3c**). Note that significant non-uniformity exists (different parts of the film show different amounts of current generation), which could be attributed to 2D phases containing different n values as indicated by the optical absorption results (**Figure S10**).

Figure 3d compares the typical TRMC transients with 640-nm laser excitation at an intensity near 1×10^{10} cm^{-2} absorbed photon flux. The carrier generation yield is about unity for n=5 2D PSCs in this study, so the yield-mobility product $\varphi\Sigma\mu$ value can be seen as a measure of the carrier mobility. Analysis of these TRMC results yields a peak value of ~7 cm^2 $V^{-1}s^{-1}$ for the $(PEA)_2MA_4Pb_5I_{16}$ films and a higher value of ~9 cm^2 $V^{-1}s^{-1}$ for $(F\text{-}PEA)_2MA_4Pb_5I_{16}$. TRPL measurements (**Figure S11**) show carrier lifetimes of about 20 ns and 30 ns for the $(PEA)_2MA_4Pb_5I_{16}$ and $(F\text{-}PEA)_2MA_4Pb_5I_{16}$ films, respectively. TRPL carrier lifetimes of several nanoseconds are characteristic for layered organic-inorganic perovskites.[33,34] The improved carrier mobility and lifetime further confirm that the fluorine substitution can enhance charge transport and suppress recombination.[35,36] The improved photophysical properties are also consistent with a reduced dark carrier density[21] ($n_d = 6.4\times10^{16}$ cm^{-3}) for the $(F\text{-}PEA)_2MA_4Pb_5I_{16}$ sample compared to the $(PEA)_2MA_4Pb_5I_{16}$ sample ($n_d = 9.5\times10^{16}$ cm^{-3}), as shown in **Figure S12**.

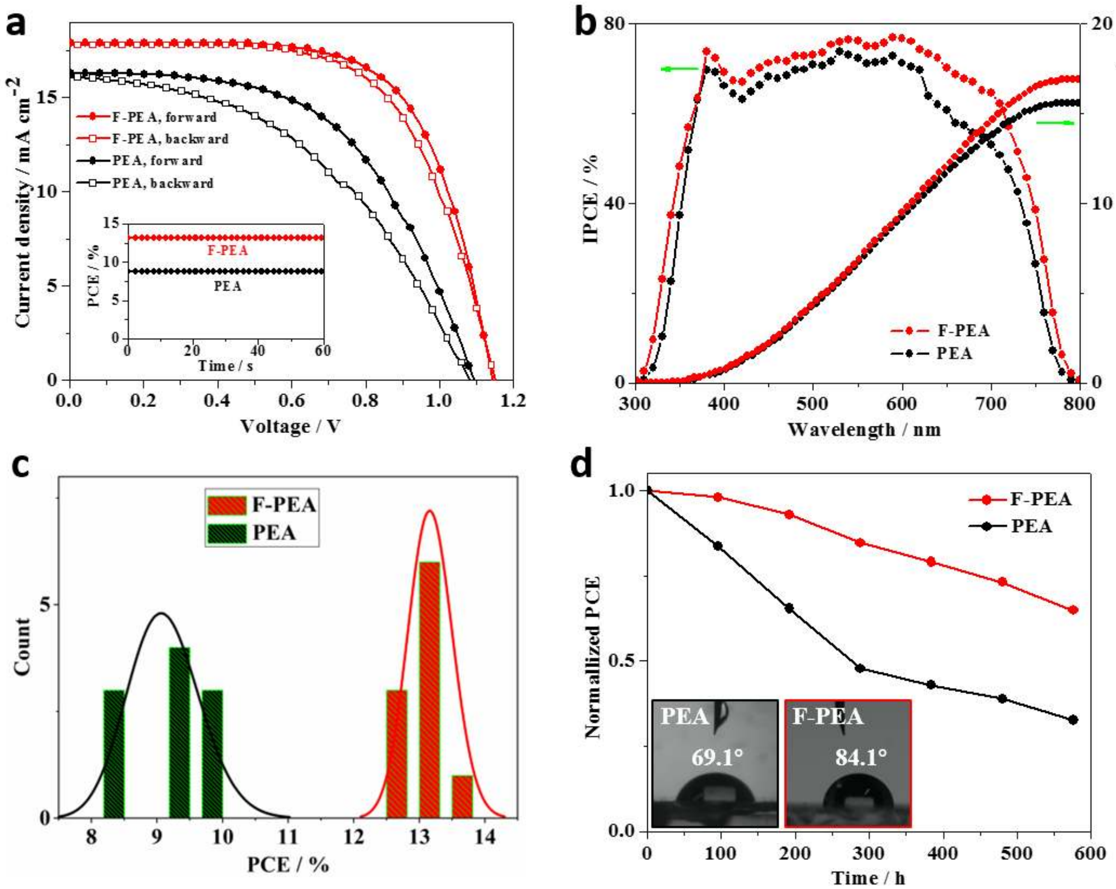

Figure 4. (**a**) J–V curves of PSCs based on n=5 2D $(PEA)_2MA_4Pb_5I_{16}$ and $(F\text{-}PEA)_2MA_4Pb_5I_{16}$ films with a bias step of 10 mV. Inset shows the stabilized power output of the corresponding devices. (**b**) IPCE spectra and integrated current curves of the corresponding devices. (**c**) Reproducibility of PSCs based on the corresponding films. (**d**) Thermal stability comparison of PEA- and F-PEA-based PSCs tested at 70°C in ambient environment, dark storage, without any encapsulation. Inset shows the contact angles between corresponding perovskite films and water.

Based on this collection of data, we anticipate that the improved structural and corresponding optoelectronic properties of the $(F\text{-}PEA)_2MA_4Pb_5I_{16}$ should contribute to the enhanced PCE in the corresponding PSCs. To test this hypothesis, we compared how the 2D cations affect the PV properties of PSCs based on n=5 2D perovskites. **Figure 4a** shows the J–V curves of $(F\text{-}PEA)_2MA_4Pb_5I_{16}$- and $(PEA)_2MA_4Pb_5I_{16}$-based PSCs under simulated AM 1.5G one-sun illumination. The corresponding PV parameters are summarized in **Table S3**. The device based on $(PEA)_2MA_4Pb_5I_{16}$ perovskite gives a PCE of 9.66%, with a J_{sc} of 16.27 mA cm^{-2}, V_{oc} of 1.10

V, and FF of 0.54, which is already among the highest PCEs of $PEA_2MA_{n-1}Pb_nI_{3n+1}$ (n ≤5) based on devices without using any additives. For $(F\text{-}PEA)_2MA_4Pb_5I_{16}$ based PSCs, the PCE is further improved to 13.64%, with a J_{sc} of 17.86 mA cm^{-2}, V_{oc} of 1.14 V, and FF of 0.67. We ascribe the improved PCE (especially the enhanced FF) with the $(F\text{-}PEA)_2MA_4Pb_5I_{16}$ perovskite thin films primarily to the improved charge transport and reduced trap density.[37,38] In addition, the PCE is also consistent with that obtained from the stabilized power outputs measurements (inset of **Figure 4a**), and J_{sc} is matched with the integrated current densities estimated from the IPCE spectra (**Figure 4b**). In addition to the improved PCE, the hysteresis (the difference in the PCEs from the reverser-scan and the forward-scan J–V curves) is also significantly reduced for PSCs based on F-PEA, which can be attributed to the improved perovskite film quality (e.g., larger grain size, lower defect density, higher carrier mobility).[36,39,40] The statistical PCE data of the PSCs based on the $(F\text{-}PEA)_2MA_4Pb_5I_{16}$ and $(PEA)_2MA_4Pb_5I_{16}$ thin films are shown in **Figure 4c**.

Thermal stability tests under an ambient environment at 70 °C for PEA- and F-PEA-based PSCs without encapsulation were also conducted. As shown in **Figure 4d**, the unencapsulated $(F\text{-}PEA)_2MA_4Pb_5I_{16}$-based devices maintained 65% of their initial PCE after 576 h; under the same conditions, the measured PCEs decreased to 32% of their initial values for $(PEA)_2MA_4Pb_5I_{16}$-based PSCs. The enhanced stability of $(F\text{-}PEA)_2MA_4Pb_5I_{16}$-based PSCs can also be seen from **Figure S13**. The color of $(F\text{-}PEA)_2MA_4Pb_5I_{16}$-based solar cells remains persistent, whereas those of $(PEA)_2MA_4Pb_5I_{16}$-based solar cells turned almost transparent. The improved environmental stability of the F-PEA-based 2D perovskites is consistent with the better hydrophobicity by fluorination (**Figure 4d inset**), lower trap densities and stronger interaction between interlayers.[5,30,35,38,41-43]

In summary, we report a simple approach of modifying PEA with fluorine to get 4-fluoro-phenethylammonium (F-PEA) and applied it in 2D perovskite solar cells. The shorter average ring centroid-centroid distances in the organic layer enhance the orbital interactions across the inorganic layers, leading to more efficient charge transport between neighboring inorganic layers. The simple fluorination of PEA cations aligns stacking of perovskite sheets and allows for a better interlayer electronic coupling. F-PEA-based 2D perovskite ($(F\text{-}PEA)_2MA_{n-1}Pb_nI_{3n+1}$, n=5) exhibited better charge transport and lower trap density than materials based on PEA. A solar cell PCE > 13% was obtained based on $(F\text{-}PEA)_2MA_4Pb_5I_{15}$, which is higher than that of PEA. This was achieved without using any additives or heated substrate to help growth of 2D perovskites. In addition, the devices based on F-PEA also displayed better stability than that based on PEA after 576 h under 70°C in an ambient environment. This promising approach provides a simple route for designing 2D PSCs with high efficiency and stability.

Acknowledgements

The work was supported by the U.S. Department of Energy under Contract No. DE-AC36-08GO28308 with Alliance for Sustainable Energy, Limited Liability Company (LLC), the Manager and Operator of the National Renewable Energy Laboratory. We acknowledge the support on perovskite synthesis and device fabrication/characterization, and microwave cavity modeling and characterization from the Hybrid Perovskite Solar Cell Program of the National Center for Photovoltaics, funded by the U.S. Department of Energy, Office of Energy Efficiency and Renewable Energy, Solar Energy Technologies Office; the support of the in-plane and out-of-plane transport measurement and analysis from the Center for Hybrid Organic Inorganic Semiconductors for Energy (CHOISE), an Energy Frontier Research Center funded by the Office of Basic Energy Sciences, Office of Science within the U.S. Department of Energy; and the support on in density functional theory calculations by supercomputer time awarded through PRACE on the Swiss National Supercomputing Centre (CSCS) under project pr51. The views expressed in the article do not necessarily represent the views of the DOE or the U.S. Government.

References

[1] Kojima, A.; Teshima, K.; Shirai, Y.; Miyasaka, T. Organometal Halide Perovskites as Visible-Light Sensitizers for Photovoltaic Cells, *J. Am. Chem. Soc.* 2009, 131, 6050–6051.

[2] NREL. Best Research-Cell Efficiencies,

http://www.nrel.gov/ncpv/images/efficiency_chart.jpg . (October 2018)

[3] Bi, D.; Yi, C.; Luo, J.; Decoppet, J.-D.; Zhang, F.; Zakeeruddin, S. M.; Li, X.; Hagfeldt, A.; Grätzel, M. Polymer-Templated Nucleation and Crystal Growth of Perovskite Films for Solar Cells with Efficiency Greater than 21%, *Nat. Energy*, 2016, 1, 16142.

[4] Zhang, F.; Shi, W.; Luo, J.; Pellet, N.; Yi, C.; Li, X.; Zhao, X.; Dennis, T.J.S.; Li, X.; Wang, S.; Xiao, Y.; Zakeeruddin, S.M.; Bi, D.; Grätzel, M. Isomer-Pure Bis-PCBM-Assisted Crystal Engineering of Perovskite Solar Cells Showing Excellent Efficiency and Stability, *Adv. Mater.*, 2017, 29, 1606806.

[5] Zhang, F.; Bi, D. Q.; Pellet, N.; Xiao, C. X.; Li, Z.; Berry, J. J.; Zakeeruddin, S. M.; Zhu, K.; Grätzel, M. Suppressing Defects Through Synergistic Effect of Lewis Base and Lewis Acid for Highly Efficient and Stable Perovskite Solar Cells, *Energy Environ. Sci.* 2018, 11, 3480−3490.

[6] Zhang, F.; Kim, D.H.; Zhu, K. 3D/2D Multidimensional Perovskites: Balance of High Performance and Stability for Perovskite Solar Cells, *Current Opinion in Electrochemistry*, 2018, 11, 105−113.

[7] Yang, S.; Wang, Y.; Liu, P.; Cheng, Y.-B.; Zhao, H.J.; Yang, H.G. Functionalization of Perovskite Thin Films with Moisture-Tolerant Molecules, *Nat. Energy*, 2016, 1, 15016.

[8] Quan, L.N.; Yuan, M.; Comin, R.; Voznyy, O.; Beauregard, E. M.; Hoogland, S.; Buin, A.; Kirmani, A.R.; Zhao, K.; Amassian, A.; Kim, D.H.; Sargent, E. H. Ligand-Stabilized Reduced-Dimensionality Perovskites, *J. Am. Chem. Soc.* 2016, 138, 2649–2655.

[9] Proppe, A. H.; Quintero-Bermudez, R.; Tan, H.; Voznyy, O.; Kelley, S. O.; Sargent, E. H. Synthetic Control over Quantum Well Width Distribution and Carrier Migration in Low-Dimensional Perovskite Photovoltaics. *J. Am. Chem. Soc.* 2018, 140, 2890−2896.

[10] Zhang, X. Q.; Wu, G.; Fu, W. W.; Qin, M. C.; Yang, W. T.; Yan, J. L.; Zhang, Z.Q.; Lu, X. H.; Chen, H. Z. Orientation Regulation of Phenylethylammonium Cation Based 2D Perovskite Solar Cell with Efficiency Higher Than 11%, *Adv. Energy Mater.* 2018, 8, 1702498.

[11] Fu, W. F.; Wang, J.; Zuo, L. J.; Gao, K.; Liu, F.; Ginger, D.S.; Jen, A.K.-Y. Two-Dimensional Perovskite Solar Cells with 14.1% Power Conversion Efficiency and 0.68% External Radiative Efficiency, *ACS Energy Lett.*, 2018, 3, 2086–2093.

[12] Zhang, X.; Wu, G.; Yang, S.; Fu, W.; Zhang, Z.; Chen, C.; Liu, W.; Yan, J.; Yang, W.; Chen, H. Vertically Oriented 2D Layered Perovskite Solar Cells with Enhanced Efficiency and Good Stability, *Small* 2017, 13, 1700611.

[13] Ma, C.Q.; Shen, D.; Ng, T-W.; Lo, M. F.; Lee, C. S. 2D Perovskites with Short Interlayer Distance for High-Performance Solar Cell Application, *Adv. Mater*. 2018, 30, 1800710.

[14] Lai, H.T.; Kan, B.; Liu, T.T.; Zheng, N.; Xie, Z. Q.; Zhou, T.; Wan, X. J.; Zhang, X.D.; Liu, Y.S.; Chen, Y. S. Two-Dimensional Ruddlesden–Popper Perovskite with Nanorod-like Morphology for Solar Cells with Efficiency Exceeding 15%, *J. Am. Chem. Soc*. 2018 140 (37), 11639−11646.

[15] Qing, J.; Liu, X.-K.; Li, M.; Liu, F.; Yuan, Z.; Tiukalova, E.; Yan, Z.; Duchamp, M.; Chen, S.; Wang, Y.; et al. Aligned and Graded Type- II Ruddlesden-Popper Perovskite Films for Efficient Solar Cells. *Adv. Energy Mater.* 2018, 8, 1800185.

[16] Tsai, H.; Nie, W.; Blancon, J.C.; Stoumpos, C.C.; Asadpour, R.; Harutyunyan, B.; Neukirch, A.J.; Verduzco, R.; Crochet, J.J.; Tretiak, S.; Pedesseau, L.; Even, J.; Alam, M.A.; Gupta, G.; Lou, J.; Ajayan, P.M.; Bedzyk, M.J.; Kanatzidis, M.G. High-Efficiency Two-Dimensional Ruddlesden–Popper Perovskite Solar Cells, *Nature*, 2016, 536, 312−316

[17] Zhang, X.; Ren, X.; Liu, B.; Munir, R.; Zhu, X.; Yang, D.; Li, J.; Liu, Y.; Smilgies, D.-M.; Li, R.; Yang, Z.; Niu, T. ; Wang, X.; Amassian, A. Zhao, K.; Liu, S. Stable High Efficiency Two-Dimensional Perovskite Solar Cells via Cesium Doping, *Energy Environ. Sci.*, 2017, 10, 2095–2102.

[18] Yan, L.; Hu, J.; Guo, Z.K.; Chen, H.; Toney, M.F.; Moran, A.M.; You, W. General Post-Annealing Method Enables High-Efficiency Two-Dimensional Perovskite Solar Cells, *ACS Appl. Mater. Interfaces*, 2018, 10, 33187-33197.

[19] Cheng, P. R.; Xu, Z.; Li, J. B.; Liu, Y. C.; Fan, Y. Y.; Yu, L.Y.; Smilgies, D. M.; Müller, C.; Zhao, K.; Liu, S.Z. Frank. Highly Efficient Ruddlesden–Popper Halide Perovskite $PA_2MA_4Pb_5I_{16}$ Solar Cells, *ACS Energy Letters* 2018, 3 (8), 1975−1982.

[20] Kikuchi, K.; Takeoka, Y.; Rikukawa, M.; Sanui, K. Structure and Optical Properties of Lead Iodide Based Two-Dimensional Perovskite Compounds Containing Fluorophenethylamines, *Current Applied Physics*.2004, 4, 599–602.

[21] Reid, O. G.; Moore, D. T.; Li, Z.; Zhao, D.;Yan, Y.; Zhu, K.; Rumbles, G. Quantitative analysis of time-resolved microwave conductivity data. *Journal of Physics D: Applied Physics*,2017, 50, 493002.

[22] Savenije, T. J.; Ferguson, A. J.; Kopidakis, N.; Rumbles, G. Revealing the Dynamics of Charge Carriers in Polymer:Fullerene Blends Using Photoinduced Time-Resolved Microwave Conductivity. *The Journal of Physical Chemistry C*, 2013, 117, 24085–24103.

[23] Carsten, B.; Szarko, J. M.; Son, H. J.; Wang, W.; Lu, L.; He, F.; Rolczynski, B. S.; Lou, S. J.;

Chen, L. X.; Yu, L. Examining the Effect of the Dipole Moment on Charge Separation in Donor–Acceptor Polymers for Organic Photovoltaic Applications, *J. Am. Chem. Soc*. 2011, 133, 20468−20475.

[24] Schroeder, B. C.; Huang, Z.; Ashraf, R. S.; Smith, J.; D'Angelo, P.; Watkins, S. E.; Anthopoulos, T. D.; Durrant, J. R.; McCulloch, I. Silaindacenodithiophene-Based Low Band Gap Polymers—The Effect of Fluorine Substitution on Device Performances and Film Morphologies, *Adv. Funct. Mater.* 2012, 22, 1663−1670.

[25] Zhang, Q. Q.; Kelly, M. A.; Bauer, N.; You, W. The Curious Case of Fluorination of Conjugated Polymers for Solar Cells, *Acc. Chem. Res*. 2017, 50, 2401−2409.

[26] Tumbleston, J. R.; Collins, B. A.; Yang, L.; Stuart, A. C.; Gann, E.; Ma, W.; You, W.; Ade, H. The Influence of Molecular Orientation on Organic Bulk Heterojunction Solar Cells, *Nat. Photonics*, 2014, 8, 385−391.

[27] http://www.jbc.org/content/273/25/15458.full.pdf.

[28] Mas-Torrent, M.; Hadley, P.; Bromley, S. T.; Ribas, X.; Tarre´s, J.; Mas, M.; Molins, E.; Veciana, J.; Rovira, C. Correlation between Crystal Structure and Mobility in Organic Field-Effect Transistors Based on Single Crystals of Tetrathiafulvalene Derivatives. *J. Am. Chem. Soc.* 2004, 126,8546−8553.

[29] Coropceanu, V.; Cornil, J.; da Silva, D. A.; Olivier, Y.; Silbey, R.; Bredas, J. L. Charge Transport in Organic Semiconductors, *Chem. Rev.* 2007, 107 (4), 926−952.

[30] Mao, L.; Ke, W.; Pedesseau, L.; Wu, Y.; Katan, C.; Even, J.; Wasielewski, M. R.; Stoumpos, C. C.; Kanatzidis, M. G. Hybrid Dion−Jacobson 2D Lead Iodide Perovskites. *J. Am. Chem. Soc.* 2018,140, 3775−3783.

[31] Mao, L.; Stoumpos, C. C.; Kanatzidis. M. G. Two-Dimensional Hybrid Halide Perovskites: Principles and Promises, *J. Am. Chem. Soc*. 2018, DOI: 10.1021/jacs.8b10851.

[32] Mitzi, D. B.; Feild, C. A.; Harrison, T. A.; Guloy, A. M. Conducting Tin Halides with a Layered Organic-Based Perovskite Structure, *Natur*e, 1994, 369, 467−469,

[33] Dohner, E. R.; Jaffe, A.; Bradshaw, L. R.; Karunadasa, H. I. Intrinsic White-Light Emission from Layered Hybrid Perovskites. *J. Am. Chem. Soc.* 2014, 136, 13154−13157.

[34] Kitazawa, N.; Watanabe, Y. Optical Properties of Natural Quantum-Well Compounds $(C_6H_5\text{-}C_nH_{2n}\text{-}NH_3)_2PbBr_4$ (n = 1−4). *J. Phys. Chem. Solids* 2010, 71, 797−802.

[35] Zhu, H.; Zhang, F.; Xiao, Y.; Wang S.; Li, X. Suppressing Defects Through Thiadiazole Derivatives that Modulate $CH_3NH_3PbI_3$ Crystal Growth for Highly Stable Perovskite Solar Cells under Dark Conditions, *J. Mater. Chem. A*, 2018, 6, 4971–4980.

[36] Yuan, Y.; Huang, J. S. Ion Migration in Organometal Trihalide Perovskite and Its Impact on Photovoltaic Efficiency and Stability, *Acc. Chem. Res.* 2016, 49, 286–293.

[37] Chen, Y. N.; Sun, Y. Y.; Peng, J. J.; Tang, J. H.; Zheng, K. B.; Liang, Z. Q. 2D Ruddlesden–Popper Perovskites for Optoelectronics, *Adv. Mater.* 2018, 30, 1703487.

[38] Frost, J. M.; Butler, K. T.; Brivio, F.; Hendon, C. H.; van Schilfgaarde, M.; Walsh, A. Atomistic Origins of High-Performance in Hybrid Halide Perovskite Solar Cells. *Nano Lett*. 2014, 14, 2584−2590.

[39] Sun, M.; Zhang, F.; Liu, H.; Li, X.; Xiao, Y.; Wang, S. Tuning the Crystal Growth of Perovskite Thin-Films by Adding the 2-pyridylthiourea Additive for Highly Efficient and Stable Solar Cells Prepared in Ambient Air, *J. Mater. Chem. A*, 2017, 5, 13448−13456.

[40] Zhao, H.; Wang, S.; Sun, M.; Zhang, F.; Li, X.; Xiao, Y. Enhanced Stability and Optoelectronic Properties of $MAPbI_3$ Films with Cationic Surface Active Agent for Perovskite Solar Cells. *J. Mater. Chem. A*, 2018, 6, 10825−10834.

[41] Zhang, F.; Wang, S.; Zhu, H.; Liu, X.; Liu, H.; Li, X.; Xiao, Y.; Zakeeruddin, S. M.; Gratzel, M. Impact of Peripheral Groups on Phenothiazine-Based Hole-Transporting Materials for Perovskite Solar Cells. *ACS Energy Lett*. 2018, 3, 1145−1152.

[40] Guo, J. J.; Bai, Z. C.; Meng, X. F.; Sun, M. M.; Song, J. H.; Shen, Z. S.; Ma, N.; Chen, Z. L.; Zhang, F. Novel Dopant-Free Metallophthalocyanines Based Hole Transporting Materials for Perovskite Solar Cells: The Effect of Core Metal on Photovoltaic Performance. *Sol. Energy* 2017, 155, 121−129.

[42] Zhang, F.; Zhao, X. M.; Yi, C. Y.; Bi, D. Q.; Bi, X. D.; Wei, P.; Liu, X. C.; Wang, S. R.; Li, X. G.; Zakeeruddin, S. M.; et al. Dopant Free Star-Shaped Hole-Transport Materials for Efficient and Stable Perovskite Solar Cells. *Dyes Pigm*. 2017, 136, 273−277.

[43] Zhang, F.; Wang, Z. Q.; Zhu, H. W.; Pellet, N.-P.; Luo, J. S.; Yi, C. Y.; Liu, X. C.; Liu, H. L.; Wang, S. R.; Li, X. G.; et al. Over 20% PCE Perovskite Solar Cells with Superior Stability Achieved by Novel and Low-Cost Hole-Transporting Materials. *Nano Energy* 2017, 41,469−475.